Thermoelectric properties of bulk multi-walled carbon nanotube - poly(vinylidene fluoride) nanocomposites: Study of the structure/property relationships

Jean-Francois Brun, Corinne Binet, Jean-Francois Tahon, Ahmed Addad, Pauline Tranchard, Sophie Barrau

Thermoelectric properties of bulk multi-walled carbon nanotube - poly(vinylidene fluoride) nanocomposites: study of the structure/property relationships

Jean-François Brun*, Corinne Binet, Jean-François Tahon, Ahmed Addad, Pauline Tranchard, Sophie Barrau

Univ. Lille, CNRS, INRAE, Centrale Lille, UMR 8207 - UMET - Unité Matériaux et Transformations, F-59000 Lille, France

*Corresponding author

E-mail address: jean-francois.brun@univ-lille.fr (J.-F. Brun)

Abstract

The cross-plane thermoelectric properties of multi-walled carbon nanotubes-poly(vinylidene fluoride) (MWCNT-PVDF) nanocomposites were investigated at room temperature as a function of MWCNT content (from 5 to 50 wt%). Special attention was paid to the influence of the nature of the polymer crystal phase. Incorporation of MWCNT induces PVDF polar β-phase formation, coexisting with the major non polar α-phase. Significant improvement of the thermoelectric properties is evidenced, with the best values obtained at 50 wt% MWCNT loading. A post treatment at high temperature (T = 165 °C) results in the development of the polar γ-phase from the α- and β-polymorphs. Nanocomposites annealing significantly enhances the Seebeck coefficient, typically from 14 up to 20 µV K^{-1}, yielding a power factor of 4.6 x 10^{-2} µW m^{-1} K^{-2} and a figure of merit ZT of 1.6 x 10^{-5} at 50 wt%, which is the best ZT value that can be found in the literature, regarding MWCNT-PVDF bulk nanocomposites. Structural analysis underlines for the first time the impact of the polymer polar γ-phase on the nanocomposite thermoelectric properties.

Keywords: carbon nanotubes, polymer-matrix composites, thermoelectric properties, polymer crystal phase

1 Introduction

Polymer based composites, loaded with conductive nanofillers, have recently emerged as a promising cost effective solution for low temperature (T < 500 K) thermoelectric applications, dedicated to waste heat conversion into electricity [1,2]. A thermoelectric material is able to convert a thermal gradient ΔT into a voltage difference ΔV by the so-called Seebeck effect and its associated coefficient $S = -\frac{\Delta V}{\Delta T}$, but optimized efficiency requires in the meantime to maximize the dimensionless figure of merit $ZT = \frac{\sigma S^2}{\kappa} T$, where σ is the electrical conductivity, κ the thermal conductivity, and T the temperature. ZT appears indeed as the key parameter at a given temperature of the maximum efficiency η of a thermoelectric generator (TEG)

$$\eta = \frac{T_{hot} - T_{cold}}{T_{hot}} \frac{\sqrt{1 + ZT_m} - 1}{\sqrt{1 + ZT_m} + \frac{T_{cold}}{T_{hot}}}$$

where $\Delta T = T_{hot} - T_{cold}$ is the temperature difference between the hot side and the cold side, and $T_m = \frac{T_{hot} + T_{cold}}{2}$.

For almost a century, thermoelectricity has been dominated by inorganic semiconductors. Since the major contribution of Hicks and Dresselhaus in 1993 [3], the thermoelectric properties have been constantly improved, relying on material nanostructuration, implementing electronic band structure engineering and phonon scattering [4]. However good performances are mainly obtained at high temperatures, typically above 700 K, whereas most of heat waste has to be harvested below 500 K. In this lower temperature range, Bi_2Te_3 and its derivatives are the only inorganic materials able to yield ZT coefficients higher than 1 at near-ambient temperatures [4]. But due to their scarcity, potential issues on environment and health, mechanical stiffness and bad processability, this class of semiconductors is not adapted to large-scale manufacturing. Growing interest has raised during the last decade on organic or hybrid inorganic/organic semiconductors. Although intrinsically conductive polymers and their composites filled with carbon nanotubes, such as poly(3,4-ethylenedioxythiophene) polystyrene sulfonate (PEDOT), polyaniline (PANI), Poly(3-hexylthiophene-2,5-diyl) (P3HT), exhibit the best thermoelectric performances [5–9], they are quite expensive and not stable enough to weathering and UV radiation. Within this context, composites

based on non-conductive polymer matrices have emerged as a potential relevant cost-effective alternative. Carbon nanotubes - polymer based composites are especially of great interest [1] since they can offer the low thermal conductivity of the polymer matrix, the potentially high electrical conductivity of the percolating nanotube network, together with easier production at large scale at relatively lower cost. Their mechanical flexibility also allows for geometrical versatility, especially well adapted to applications such as lightweight on-board devices. Several insulating polymer composites have already been studied [1,10–16], but despite some recent advances, understanding of the structure-property relationships appears to be only in its early stages.

Among thermoplastic polymers, poly(vinylidene fluoride) (PVDF) presents a peculiar interest. PVDF (chemical formula -$(CH_2$-$CF_2)_n$-) is a semi-crystalline polymer that exhibits three main crystal phases (α, β and γ) presented in Fig. 1. Physical properties of PVDF such as dielectric, ferroelectric, piezoelectric responses are very dependent on the nature (polar or non polar) of the crystal phase. The α-phase (TGTG' chain conformation) classically obtained by cooling from the melt, is the most stable but non polar phase. The γ-phase (TTTGTTTG' chain conformation) and the β-phase (all-trans chain conformation) are both polar phases commonly induced by high temperature annealing [17–19] and by mechanical stretching [20–23] respectively.

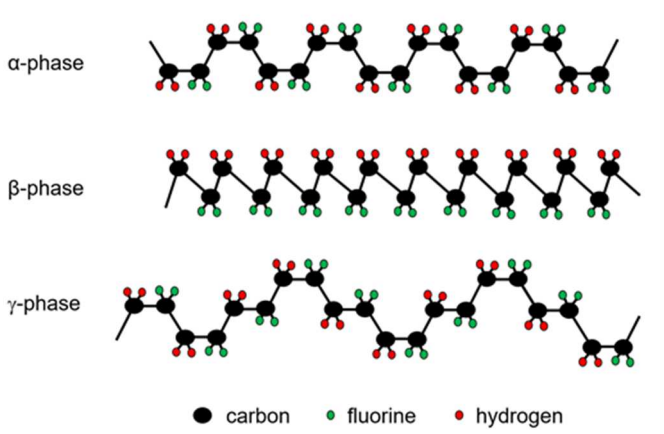

Fig. 1. Schematic representation of the chain conformation of PVDF for α, β and γ crystal phases.

Nanofiller incorporation is another way to promote one of these two polar phases [24–28]. Nanocomposites based on a PVDF matrix loaded with multi-walled carbon nanotubes (MWCNT), have been widely investigated for their piezoelectric properties

[29–32] and appear now as interesting candidates for thermoelectric applications [12,14,33–38].

In the present work, PVDF based composites, incorporating MWCNT at contents up to 50 wt%, were elaborated by a simple solution mixing process. The thermoelectric properties have been fully investigated at room temperature, before and after a thermal post treatment at 165 °C. Special attention has been paid, to our knowledge for the first time, to the influence of the polymer crystal phase on the thermoelectric properties of the composites.

2 Experimental

2.1 Materials and composites elaboration

PVDF (Kynar®720) was provided by Arkema (M_n = 80-120 kg.mol^{-1}, M_w = 200-250 kg.mol^{-1}, degree of polymerization $\overline{Xn}$ = 1500, density d = 1.78). Multi-walled carbon nanotubes (MWCNT) obtained from Nanocyl (Nanocyl 7000 series) were produced by catalytic chemical vapor deposition (CCVD). Their average diameter and length are 9.5 nm and 1.5 µm respectively. The purity is around 90 wt%. The MWCNT were used without purification. N,N-dimethylacetamide (DMAc) was purchased from Sigma-Aldrich.

The nanocomposites were elaborated by solution mixing according to the following procedure. CNT were dispersed in DMAc and sonicated for 2h at ambient temperature. PVDF was dissolved in DMAc and magnetically stirred at 70 °C. Subsequently, the two solutions were blended together, magnetically stirred and sonicated for 1 h. In order to allow solvent evaporation, the solution was poured into a silicone mold and left at room temperature under atmospheric pressure for 2 weeks. The residual solvent was removed by placing the composite material in a vacuum oven for 4 h. The material was then hot pressed at 210 °C under 50 bars. For the sake of comparison, neat PVDF sample was processed under similar conditions in order to ensure identical history. Resulting films are approximately 10 x 10 cm^2 with thicknesses ranging from 0.5 to 1 mm.

A high temperature annealing (T = 165 °C) for t = 118 h was applied to composites in order to induce the PVDF polar γ-phase. The composites are denoted NTx, where x holds for the CNT content in wt%, namely NT0 for neat PVDF, NT5, NT15, NT30 and

NT50 corresponding to a CNT content of 5, 15, 30 and 50 wt% respectively and NTxa refers to the high temperature annealed composites.

2.2 Morphology and structure of the composites

The distribution of MWCNT was investigated by field emission scanning electron microscopy (FE-SEM) and transmission electron microscopy (TEM), using respectively an Hitachi S4700 apparatus, operating at an acceleration voltage of 5 kV, and FEI TECNAI G2 operating at 200kV. The SEM micrographs were taken from the edge of cryofractured samples.

The structure of nanocomposites was studied by differential scanning calorimetry (DSC), Fourier transform infrared spectroscopy (FTIR) and Wide-Angle X-ray Scattering (WAXS). Thermal characterization was performed on a DSC Q20 (TA Instruments). DSC scans where performed between 0 and 200 °C at a heating rate of 10 °C min^{-1} under nitrogen atmosphere. The crystallinity was determined from the relation $\chi = \Delta H_f / (m\ \Delta H_f^0)$ with m the polymer fraction [39] and ΔH_f^0=93.07 J g^{-1} the melting enthalpy of 100% crystallized PVDF [40]. FTIR analysis was carried out on a Spectrum 100 spectrometer (Perkin Elmer) in ATR (Attenuated Total Reflection) mode. Data acquisition was achieved on 16 scans at a resolution of 2 cm^{-1}. WAXS experiments were performed at room temperature on a Xeuss 2.0 (Xenocs) operating under vacuum with a GeniX3D microsource (λ = 1.54 Å) at 0.6 mA and 50 kV and a 2D Pilatus 3R 200K detector. The sample-to-detector distance was 121 mm.

2.3 Thermoelectric properties measurement

All thermoelectric measurements were carried out across sample thickness at room temperature. For electrical and thermal conductivity measurements, as well as for Seebeck coefficient measurements, discs of 13 mm in diameter were cut from the films (the thickness is of 0.5 to 1 mm). It is worth mentioning that experiments have been systematically performed on the same sample for each nanotube loading.

The cross-plane electrical conductivity was measured by broadband dielectric spectroscopy (Novocontrol BDS4000). The complex relative dielectric permittivity $\varepsilon_r^*(f) = \varepsilon_r'(f) + i\varepsilon_r''(f)$ was measured from f = 10^{-1} to 10^6 Hz. The static electrical conductivity σ_{DC} is the real part of the conductivity (σ') extrapolated at 10^{-1} Hz and

calculated from the imaginary part ε_r'' using $\sigma' = 2\pi f \varepsilon_0 \varepsilon_r''$ [41], where ε_0 is the permittivity of vacuum. For comparison, the in-plane electrical conductivity was measured with a 4-point collinear probe station (Süss MicroTec + Keithley source meter) at the samples surface.

The cross-plane Seebeck coefficient (or thermoelectric power) was measured with an in-house built device (see supplementary information).

The cross-plane thermal conductivity of samples was deduced from thermal diffusivity measurements carried out with a Netzsch light flash apparatus LFA 467 HyperFlash (Netzsch-Gerätebau GmbH). In this method, the front surface of a plane-parallel sample is heated by a xenon flash lamp with energy variation (by voltage and pulse-length). The resulting temperature increase of the rear face is measured with an infrared (IR) detector. The thermal diffusivity is then calculated using optimization method: in this work, all measured curves were perfectly fitted by a Cowan model with a pulse correction. The thermal diffusivity of the sample is measured in the through-thickness direction and yields a corresponding value of the thermal conductivity κ according to the following equation $\kappa = \alpha \rho C_P$, where α is the thermal diffusivity, ρ the density and C_p the specific heat capacity. The neat PVDF sample was slightly dusted with graphite paint on both sides to ensure good absorption of the light pulse, whereas thanks to the good absorption of the carbon nanotubes, no dusting was needed for the composites.

Specific heat capacity C_p was deduced from Differential Scanning Calorimetry (DSC) measurements using a Modulated DSC Q2000 (TA Instruments). C_p of samples (weight around 15 mg) was measured at 26.85 °C after calibration with sapphire.

The density ρ of each sample was determined with a precision scale (Mettler Toledo) thanks to a kit for density determination: the sample was first weighted into air, then immersed into ethanol (Fluka, purity ≥ 99.8 %, density = 0.79 g cm^{-3}) ; the density is calculated by applying the Archimedes' principle.

Thus, the cross-plane figure of merit (ZT) and the corresponding power factor (PF) are calculated at T = 300 K as follows : $ZT = \frac{\sigma S^2}{\kappa} T$ and $PF = \sigma S^2$, using all cross-plane values.

3 Results and discussion

3.1 Morphology and structure

The distribution of carbon nanotubes in the polymer matrix was assessed by SEM observations. Fig. 2a-b shows the micrographs of the cryofractured area of nanocomposites NT5 and NT50. Aggregates of CNTs or CNT impregnated PVDF are observed homogeneously distributed in the polymer matrix. Indeed, NT5 (Fig. 2a) exhibits a high content of impregnated CNT while NT50 (Fig. 2b) presents at first sight a large number of CNT clusters. However, TEM images of NT50 (Fig2 c-d) reveal PVDF areas and impregnated CNT. For further insight, SEM and TEM images of the nanocomposites at different magnifications, before and after annealing, are reported in Fig. S2 (in supplementary information). Consequently, SEM and TEM observations are clearly indicative of a good interfacial adhesion between carbon nanotubes and the polymer matrix.

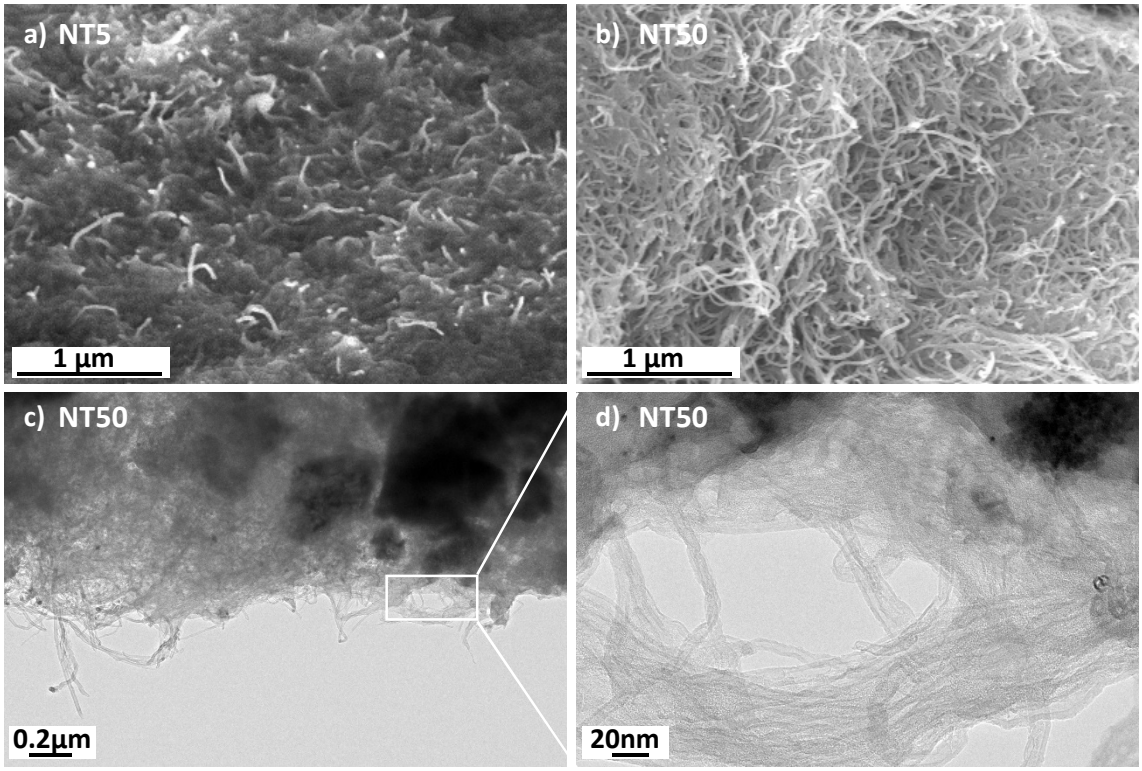

Fig. 2. SEM images of cryofractured cross-sections of (a) NT5 and (b) NT50 composites. TEM micrographs of NT50 (c and d). The image d is the magnification of the part inside the purple rectangle of image c.

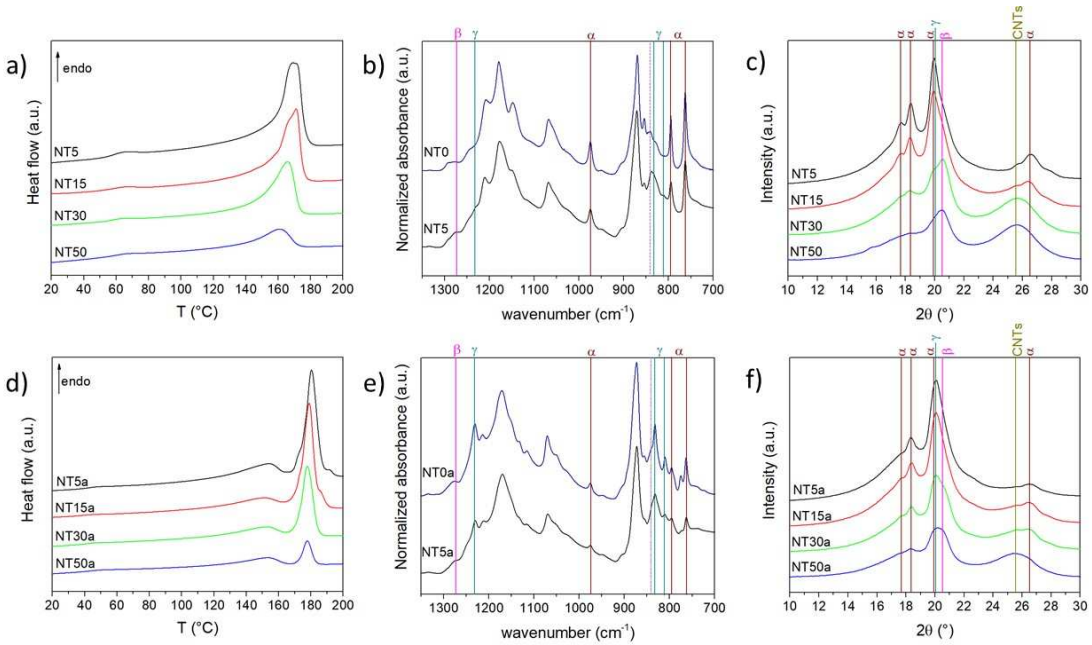

Fig. 3. a) d) DSC thermograms, b) e) FTIR spectra and c) f) WAXS intensity profile of nanocomposites NTx (a, b, c) and NTxa (d, e, f).

In nanocomposites, the impact of MWCNT on PVDF crystallinity and crystal phase was evaluated using three complementary techniques (DSC, FTIR and WAXS).

Thermograms of non-annealed nanocomposites are shown in Fig. 3a. For the sake of clarity, DSC measurements performed on NT0 are reported in Fig. S3 (in supplementary information). NT0 presents an endothermic peak associated to the melt of primary crystals at T = 165 °C. These crystals crystallized from the melt are in α-phase. At lower temperature (around T = 65 °C) a small endotherm corresponding to the melting of secondary crystals is observed. The presence of MWCNT induces a low temperature shoulder to the main peak at around T = 160 °C which might be correlated to the presence of PVDF β-phase. The crystallinity ratio (χ) of the nanocomposites is calculated assuming that the different crystal phases in PVDF have the same melting enthalpy of 100% crystallized polymer. Values of χ are reported in Table 1. The relative crystallinity of PVDF decreases with the increase of MWCNT content. This evolution can be explained by the confinement of the polymer matrix due to the high content of MWCNT which limits the PVDF crystallization.

FTIR experiments (Fig. 3b) are used to assess the PVDF crystal phases in NT0 and NT5. A detailed description of the FTIR bands is reported in Table S1 (in supplementary information). At higher CNT content, the FTIR signal is limited because of the high absorbance of nanotubes [42]. The NT0 spectrum presents the bands at 764

cm^{-1}, 795 cm^{-1} and 976 cm^{-1} characteristic of the PVDF α-phase [43,44]. Incorporation of CNT induces the presence of additional bands at 812 cm^{-1}, 833 cm^{-1} and 1234 cm^{-1} corresponding to the PVDF γ-phase and a band at 1275 cm^{-1} as a signature of the PVDF β-phase. Note that the band at 840 cm^{-1} is attributed to both γ- and β-phases. Therefore, FTIR data establishes the co-existence of the three PVDF α-, γ- and β-phases in NT5. WAXS spectra of NT0 reported in Fig. S4 (in supplementary information) exhibit characteristic peaks at 2θ = 17.6, 18.3, 19.9 and 26.5° attributed to the PVDF α-phase and corresponding to the (100), (020), (110/021) and (120) planes respectively [45]. After CNT incorporation, the diffractograms (Fig. 3c) exhibit additional peaks around 20.5° and 25.5°. The peak located at 20.5° corresponds to the PVDF β-phase with the (110/200) planes at 2θ = 20.6°. A contribution from the PVDF-γ phase with the characteristic peaks at 2θ = 18.2° and 20.1° associated to the (020) and (110/101) planes respectively may not be ruled out. The peak 2θ = 25.5° is a signature of carbon nanotubes. It corresponds to the (002) plane and is associated to the CNT inter-wall distance (d = 0.345 nm) [46]. The WAXS spectra were fitted by pseudo-Voigt functions presented in Fig. S5 (in supplementary information) in order to derive an estimate fraction (F) of the different crystal phases from the ratio of the crystal phase peak area to the total crystal peak area. The relative values of F(α), F(γ) et F(β) are reported in Table 1. The presence of CNT results in a decrease of both α and γ phases, and in an increase of the β phase content. For NT50, the γ phase fraction is null, F(β) is maximum and a fraction of α phase is still remaining.

Table 1
Degree of crystallinity (χ) and fractions (F) of the PVDF crystal phases.

	χ (%)[a]	F(α) (%)[b]	F(γ) (%)[b]	F(β) (%)[b]
NT0	79	100	-	-
NT5	81	66	14	20
NT15	76	56	12	31
NT30	75	34	5	54
NT50	70	36	-	64
NT0a	80	31	69	-
NT5a	81	34	58	7
NT15a	75	32	56	12
NT30a	76	28	46	26
NT50a	70	25	39	35

[a)] calculated by DSC, [b)] by deconvolution of WAXS diffractograms

For the same kind of MWCNT-PVDF nanocomposites, but at lower CNT content (< 1.2 wt%), we have already reported the formation of a high fraction (around 45%) of PVDF γ-phase induced by the presence of carbon nanotubes with a maximum value reached at 0.7 wt% [47]. The present decrease in γ-fraction at higher content is in agreement with the behavior previously reported. The fraction of β-phase significantly increases with the content of CNT aggregates due to local interactions in nanocomposites. The CF groups of PVDF interacts with carbon nanotubes by hydrophobic-hydrophobic interactions. The change in PVDF crystal polymorph from α to β due to the presence of multi-walled carbon nanotubes has already been reported in literature [48].

In order to probe the influence of the polymer crystal phase on the thermoelectric properties, all samples were annealed at 165 °C for 118 h, to promote the PVDF polar γ-phase [18,19]. The same characterization procedures were carried out by DSC, WAXS and FTIR on the annealed samples. The thermograms of nanocomposites (Fig. 3d) exhibit a shift in the main peak towards higher temperature corresponding to the presence of PVDF γ-phase. The low temperature contribution is associated to the remaining α-phase. For comparison, the thermograms of the nanocomposites before and after annealing were reported in Fig S3 (in supplementary information). The annealing step does not significantly impact the total crystallinity of the nanocomposites, as reported in Table 1. The signature of γ-phase formation induced by the high temperature annealing is observed in Fig. 3e with the large FTIR band at 1234 cm^{-1}. As previously observed a fraction of α-phase is still present. Moreover both samples NT0a and NT5a have a small band at 1275 cm^{-1} characteristic of β-crystal phase. In Fig. S4 (in supplementary information), the WAXS intensity profile of NT0a mainly exhibits the characteristic peaks of PVDF γ-phase. The mechanism of formation of the γ-phase is complex and has been detailed by Prest *et al.* [18]. After CNT incorporation, the diffractograms (Fig. 3f) present additional peaks associated to β-phase. The fractions F(α), F(γ) et F(β) obtained according to the same fitting procedure are reported in Table 1. The presence of MWCNT aggregates induces the formation of the PVDF polar β-phase associated to a decrease in both α and γ-phase contents, as observed for non-annealed composites.

To sum up, for both kinds of nanocomposites (NTx and NTxa), owing to the existence of favorable interactions between the surface of carbon nanotube aggregates and the polymer chains, the formation of the polar β-phase is favored. The high temperature annealing induces the formation of a significant fraction of PVDF polar γ-phase from both α- and β-phases and does not affect the overall crystallinity of nanocomposites. Therefore, in annealed samples, the main PVDF crystal phases are the polar γ- and β-phases with a clear predominance of the γ-phase.

3.2 Thermoelectric properties

Fig. 4a shows the cross-plane as well as the in-plane electrical conductivity (σ) of the samples as a function of MWCNT weight fraction, before and after annealing. As expected, all composites are electrically conductive. The percolation threshold (pc) is obviously reached below 5 wt% MWCNT content, which is in good agreement with previous work (pc < 1 wt%) [47]. The cross-plane conductivity is 4.0 10^{-11} S m^{-1} for NT0 and reaches 9.0 10^{-2} S m^{-1} for NT5 and 2.2 10^{2} S m^{-1} for NT50.

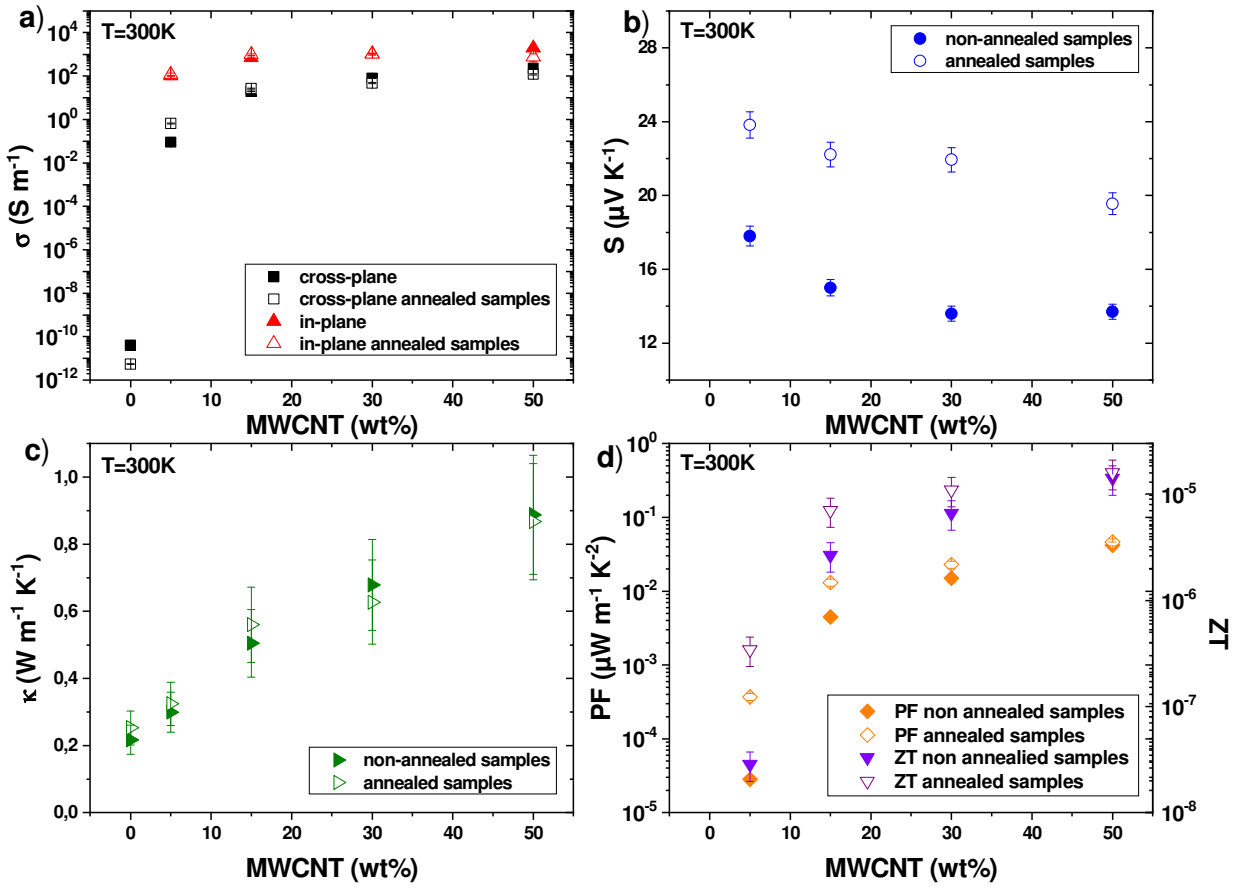

Fig. 4. a) cross-plane (square) and in-plane (up triangle) electrical conductivity (σ), b) cross-plane Seebeck coefficient (S), c) cross-plane thermal conductivity (κ) and d) cross-plane power factor (PF) (diamond) and figure of merit (ZT) (down triangle) as a function of MWCNT content; plain symbols are for NTx and open symbols for NTxa.

These values, reported in Table 2, are much higher than those obtained by Sun *et al.* [12] for composites elaborated by a melt blending process ($\sigma = 8.0\ 10^{-3}$ S m^{-1} for NT5), but also by Du *et al.* [14] for porous composites elaborated by solvent vapor-induced phase separation ($\sigma = 16.0$ S m^{-1} at NT15), confirming the relevance of our elaboration process. Nevertheless, they are lower than those obtained by Krause *et al.* [16] ($\sigma = 3.2$ S m^{-1} for NT2) for samples prepared by melt mixing and compression molding, but the corresponding resistivity was measured with a 4-wires technic and at 40 °C. In this work the in-plane electrical conductivity measured on the sample surface by a 4-point collinear probe appears 10 to 100 times higher than the cross-plane values obtained by dielectric spectroscopy (Fig. 4a), clearly indicating that thermoelectric properties of composites are highly anisotropic. Electrical anisotropy is a well-known phenomenon regarding polymer-based composites filled with carbon nanotubes [49] and seems mainly due to the elaboration process. In the present work, it can be supposed that melt molding during nanocomposite fabrication produces slight tilting of nanotubes at the surface of both sides of films, creating new contacts between tubes, thus enhancing the in-plane electrical conductivity. It seems thus important to recall that, in order to accurately evaluate the thermoelectric performance of a material, the parameters (σ), (S) and (κ) must be evaluated along the same direction as the temperature gradient. In the present case, evaluating the final figure of merit (ZT) with these in-plane electrical conductivities would yield to an overestimation of 1 to 2 orders of magnitude. To fully characterize the in-plane thermoelectric properties, an appropriate calculus of the figure of merit (ZT) would require a measurement of the in-plane Seebeck coefficient and thermal conductivity, by the 3 omega technique for example.

Table 2
Cross-plane electrical conductivity (σ), Seebeck coefficient (S), thermal conductivity (κ), power factor (PF) and figure of merit (ZT) of nanocomposites.

	σ (S m^{-1})	S (μV K^{-1})	κ (W m^{-1} K^{-1})	PF (μW m^{-1} K^{-2})	ZT (T=300K)
NT0	4. 0 x 10^{-11}	--	0.22	--	--
NT5	9.0 x 10^{-2}	18	0.30	2.9 x 10^{-5}	2.9 x 10^{-8}
NT15	2.0 x 10^{1}	15	0.51	4.5 x 10^{-3}	2.7 x 10^{-6}
NT30	8.1 x 10^{1}	14	0.68	1.5 x 10^{-2}	6.6 x 10^{-6}
NT50	2.2 x 10^{2}	14	0.89	4.2 x 10^{-2}	1.4 x 10^{-5}
NT0a	5.5 x 10^{-12}	--	0.25	--	--
NT5a	6.6 x 10^{-1}	24	0.32	3.7 x 10^{-4}	3.4 x 10^{-7}
NT15a	2.7 x 10^{1}	22	0.56	1.3 x 10^{-2}	7.0 x 10^{-6}
NT30a	4.8 x 10^{1}	22	0.63	2.3 x 10^{-2}	1.1 x 10^{-5}
NT50a	1.2 x 10^{2}	20	0.87	4.6 x 10^{-2}	1.6 x 10^{-5}

The values of electrical conductivity measured before and after annealing are, as expected, pretty similar suggesting that the polymer crystal phases have a limited impact on the electrical properties. Since the PVDF matrix is non-conductive and because the percolation threshold of composites is far exceeded, electrical conductivity is only due to MWCNT network, and more specifically to direct contacts between nanotubes, often mentioned as "ohmic conduction".

Fig. 4b shows the Seebeck coefficient values (S) of the composites. All values are positive, meaning that the majority of the charge carriers are holes, which is consistent with the known p-type semiconducting behavior of MWCNT bundles [50]. A decrease of (S) with increasing filler content is observed, from 18 down to 14 μV K^{-1} for non-annealed samples, and from 24 down to 19 μV K^{-1} for annealed samples, which shows that the annealing treatment increases the S values at a given filler fraction. These values are greater than those already observed for MWCNT – polymer composites which stand mostly between 10 and 14 μV K^{-1} or even below [15,16], except the unique value of 325 μV K^{-1} obtained by Du *et al.* at 15 wt% MWCNT loading [14]. This behavior is consistent with the empirical trend generally observed in organic thermoelectrics, where (S) decreases as (σ) increases [51]. As can be seen, the S values are significantly improved by the presence of the polar γ-phase (Table 1). For non-annealed, as well as for annealed samples, the best value is obtained at 5 wt% of MWCNT, which corresponds, in both cases, to the highest content of γ-phase. The values then decrease with increasing MWCNT fraction while the γ-phase fraction

decreases. Thus, the annealed samples exhibit from 30% up to 45% higher Seebeck values than those of non-annealed samples. The explanation is to be found into electronic band structure modifications and thus, remains complex for such heterogeneous systems. The Seebeck coefficient is by definition strongly related to the electrical conductivity through the density of states (DOS). But, while the electrical conductivity is related to the number of charge carriers having an energy close to the Fermi level, the Seebeck coefficient is related to an asymmetric shape of DOS around this Fermi level [51]. It can then be assumed that the polar γ crystal phase of the polymer, induced by the high temperature annealing, promotes an asymmetry increase in the DOS, at the Fermi level, resulting in a direct increase of the Seebeck coefficient, decoupled from the electrical conductivity which is not affected. As previously mentioned in the 3.1 section, the mechanism of formation of the γ phase is complex. Its impact on the Seebeck coefficient, i.e., the shape of the electronic band structure at the Fermi level, is even more complex, especially since the three phases α, β, γ are competing.

Fig. 4c exhibits the thermal conductivity of the composites. A quite linear increase, by a factor 4, is observed, from 0.22 W m^{-1} K^{-1} for NT0 up to 0.89 W m^{-1} K^{-1} for NT50. The value of 0.22 is in perfect agreement with the value provided by the manufacturer Arkema. Compared to the thermal conductivity of pristine bulk MWCNT, which is around 3.0 W m^{-1} K^{-1} [50], the value of 0.89 for NT50 proves that, despite the relatively high content of nanotubes, the expected increase in thermal conductivity is moderate. Furthermore, as in the case of electrical conductivity, it can be seen that the values measured before and after annealing are almost identical, which allows to take advantage, into the figure of merit (ZT), of the increase of the Seebeck coefficient induced by the annealing treatment.

The power factor ($PF = \sigma S^2$) and the dimensionless figure of merit (ZT) have consequently been calculated and reported in Fig. 4d. As can be seen, PF and ZT follow the same trend: the values increase continuously with MWCNT content, up to 50 wt%. For non-annealed as well as for annealed samples, the increase in ZT values is governed by the exceptional increase of electrical conductivity up to 13 orders of magnitude, without much influence of the nature of the crystal phases of PVDF. Yet, it is also clearly shown that, at a given filler fraction, annealing increases the figure of merit ZT

by increasing S values ; the latter appears directly correlated to the γ-phase fraction of PVDF: the higher the fraction, the higher the Seebeck. This increasing is not always observed in nanocomposites. Indeed, Du *et al.* [14] showed a maximum for 15 wt% of MWCNT, followed by a decrease at higher filler content. Between NT5 and NT50, (PF) as well as (ZT) is enhanced by 3 orders of magnitude before annealing and by 2 orders of magnitude after annealing. The best values are those of the annealed samples confirming again the interest of the thermal treatment. The maximum values are obtained for NT50a, with PF = 4.6 10^{-2} μW m^{-1} K^{-2} and ZT = 1.6 10^{-5} which are greater than those obtained by Sun *et al.* for 8 wt% MWCNT [12] and by Krause *et al.* for 2 wt% MWCNT [16]. The present values stand among the best values reported in the literature at T = 300 K, regarding non-conductive polymer matrix based composites, filled with MWCNT, and are only topped by the great values of PF = 1.7 μW m^{-1} K^{-2} and ZT = 3.3 10^{-3} obtained by Du *et al.* on porous composites [14] and PF = 9.3 10^{-2} μW m^{-1} K^{-2} and ZT = 6.8 10^{-5} obtained by Antar *et al.* on PLA based composites [10], as shown in Table 3.

Table 3
List of the maximum thermoelectric values obtained for non-conductive polymer matrix based composites filled with MWCNTs.

Material wt% MWCNT / polymer)	$\sigma_{in\text{-}plane}$ (S m^{-1})	$\sigma_{cross\text{-}plane}$ (S m^{-1})	$S_{cross\text{-}plane}$ (μV K^{-1})	$\kappa_{cross\text{-}plane}$ (W m^{-1} K^{-1})	PF (μW m^{-1} K^{-2})	ZT (T=300K)	ZT (T=313 K)
2.5 / polycarbonate [11]	7.3		8.5	0.33	5.3 x 10^{-4}	4.8 x 10^{-7}	
18 vol% / PLA [10]	1.15 x 10^{2}		9.0	0.41	9.3 x 10^{-2}	6.8 x 10^{-5}	
2 / Poly(butylene terephthalate) (PBT) [16]	5.1		6.8	0.28	2.0 x 10^{-4}		2.7 x 10^{-7}
2 / Polypropylene (PP) [16]	1.6		9.5	0.28	1.0 x 10^{-4}		1.7 x 10^{-7}
2 / Polycarbonate (PC) [16]	8.5		8.5	0.28	6.0 x 10^{-4}		6.8 x 10^{-7}
4 / Acrylonitrile butadiene styrene (ABS) [16]	25.7		3.6	0.28	3.0 x 10^{-4}		3.8 x 10^{-7}
2 / Polyamide 66 (PA66) [16]	5.0		6.3	0.28	2.0 x 10^{-4}		2.2 x 10^{-7}
5 / cellulose film [15]	15		10	0.08	1.5 x 10^{-3}	6.0 x 10^{-6}	
5 / cellulose aerogel [15]	3.5 x 10^{-1}		11	0.03	4.2 x 10^{-5}	4.7 x 10^{-7}	
3 / PVDF [12]		2.0 x 10^{-2}	12	0.55	2.9 x 10^{-6}	1.6 x 10^{-9}	
3 / PVDF foam [12]		4.0 x 10^{-3}	8.0	0.10	2.6 x 10^{-7}	7.7 x 10^{-10}	
2 / PVDF [16]	3.2		14.3	0.28	7.0 x 10^{-4}		7.4 x 10^{-7}
50 / PVDF annealed (this work)		1.2 x 10^{2}	20	0.87	4.6 x 10^{-2}	1.6 x 10^{-5}	
50 / PVDF annealed (for comparison only, this work)	1.9 x 10^{3}		20	0.87	7.6 x 10^{-1}	2.6 x 10^{-4}	
15 / PVDF porous [14]	16		325	0.15	1.7	3.3 x 10^{-3}	

4 Conclusion

Bulk MWCNT-PVDF composites (from 5 to 50 wt%) have been elaborated by solution mixing. The room temperature thermoelectric properties (PF and ZT) were continuously enhanced at increasing filler content, thanks to an exceptional increase of 4 orders of magnitude of the electrical conductivity (σ) reaching 2.2 10^2 S m^{-1}, a slight decrease of the Seebeck coefficient (S) from 18 to 14 μV K^{-1}, and a moderate increase of the thermal conductivity (κ) from 0.22 to 0.89 W m^{-1} K^{-1}. The polymer crystal phase, mainly in α-form, is impacted by the incorporation of MWCNT which induces the development of the polar β-phase. The investigation of high temperature annealed nanocomposites, reveals that the polar γ–phase, although very slightly affecting (σ) and (κ), yields a 30% increase of (S), from 14 to 20 μV K^{-1}. The best values of (PF) and (ZT) are those of the annealed samples with 50 wt% MWCNT. These values appear higher than those of other insulated polymer based composites filled with MWCNT. Nevertheless, as previously observed in other studies, it can be expected than these values will be enhanced by 1 to 2 orders of magnitude with the use of single-walled carbon nanotubes (SWCNT) and by fabricating composite thin films (thickness < 1 μm), since in-plane properties are known to be better than cross-plane performances. This work clearly demonstrates the potential of polymer based composites for thermoelectric applications and underlines the fact that understanding the structure-property relationships is vital to enhance their performances.

Acknowledgment

Arkema (Cerdato, France) is acknowledged for the kind supply of PVDF. The SEM and WAXS facilities in Lille (Institut Chevreul) are supported by the Conseil Régional Hauts-de-France and European Regional Development Fund (ERDF). The authors would like to thank Dr Jean-Marc Lefebvre for its contribution.

References

[1] C. Yu, Y.S. Kim, D. Kim, J.C. Grunlan, Thermoelectric Behavior of Segregated-Network Polymer Nanocomposites, Nano Lett. 8 (2008) 4428–4432. https://doi.org/10.1021/nl802345s.

[2] O. Bubnova, X. Crispin, Towards polymer-based organic thermoelectric generators, Energy Environ. Sci. 5 (2012) 9345–9362. https://doi.org/10.1039/C2EE22777K.

[3] L.D. Hicks, M.S. Dresselhaus, Effect of quantum-well structures on the thermoelectric figure of merit, Phys. Rev. B. 47 (1993) 12727–12731. https://doi.org/10.1103/PhysRevB.47.12727.

[4] C. Gayner, K.K. Kar, Recent advances in thermoelectric materials, Prog. Mater. Sci. 83 (2016) 330–382. https://doi.org/10.1016/j.pmatsci.2016.07.002.

[5] C. Gao, G. Chen, Conducting polymer/carbon particle thermoelectric composites: Emerging green energy materials, Compos. Sci. Technol. 124 (2016) 52–70. https://doi.org/10.1016/j.compscitech.2016.01.014.

[6] Y. Zheng, H. Zeng, Q. Zhu, J. Xu, Recent advances in conducting poly(3,4-ethylenedioxythiophene):polystyrene sulfonate hybrids for thermoelectric applications, J. Mater. Chem. C. 6 (2018) 8858–8873. https://doi.org/10.1039/C8TC01900B.

[7] W. Fan, L. Liang, B. Zhang, C.-Y. Guo, G. Chen, PEDOT thermoelectric composites with excellent power factors prepared by 3-phase interfacial electropolymerization and carbon nanotube chemical doping, J. Mater. Chem. A. 7 (2019) 13687–13694. https://doi.org/10.1039/c9ta03153g.

[8] D. Qu, X. Li, H. Wang, G. Chen, Assembly Strategy and Performance Evaluation of Flexible Thermoelectric Devices, Adv. Sci. 6 (2019) 1900584. https://doi.org/10.1002/advs.201900584.

[9] D. Qu, X. Huang, X. Li, H. Wang, G. Chen, Annular flexible thermoelectric devices with integrated-module architecture, Npj Flex. Electron. 4 (2020) 1–7. https://doi.org/10.1038/s41528-020-0064-2.

[10] Z. Antar, J.-F. FELLER, H. Noël, P. Glouannec, K. Elleuch, Thermoelectric behavior of melt processed carbon nanotube/graphite/poly(lactic acid) conductive biopolymer nanocomposites (CPC), Mater. Lett. 67 (2012) 210–214. https://doi.org/10.1016/j.matlet.2011.09.060.

[11] M. Liebscher, T. Gärtner, L. Tzounis, M. Mičušík, P. Pötschke, M. Stamm, G. Heinrich, B. Voit, Influence of the MWCNT surface functionalization on the thermoelectric properties of melt-mixed polycarbonate composites, Compos. Sci. Technol. 101 (2014) 133–138. https://doi.org/10.1016/j.compscitech.2014.07.009.

[12] Y.-C. Sun, D. Terakita, A.C. Tseng, H.E. Naguib, Study on the thermoelectric properties of PVDF/MWCNT and PVDF/GNP composite foam, Smart Mater. Struct. 24 (2015) 085034. https://doi.org/10.1088/0964-1726/24/8/085034.

[13] L. Tzounis, M. Hegde, M. Liebscher, T. Dingemans, P. Pötschke, A.S. Paipetis, N.E. Zafeiropoulos, M. Stamm, All-aromatic SWCNT-Polyetherimide nanocomposites for thermal energy harvesting applications, Compos. Sci. Technol. 156 (2018) 158–165. https://doi.org/10.1016/j.compscitech.2017.12.030.

[14] F.-P. Du, X. Qiao, Y.-G. Wu, P. Fu, S.-P. Liu, Y.-F. Zhang, Q.-Y. Wang, Fabrication of Porous Polyvinylidene Fluoride/Multi-Walled Carbon Nanotube Nanocomposites and Their Enhanced Thermoelectric Performance, Polymers. 10 (2018) 797. https://doi.org/10.3390/polym10070797.
[15] M. Gnanaseelan, Y. Chen, J. Luo, B. Krause, J. Pionteck, P. Pötschke, H. Qi, Cellulose-carbon nanotube composite aerogels as novel thermoelectric materials, Compos. Sci. Technol. 163 (2018) 133–140. https://doi.org/10.1016/j.compscitech.2018.04.026.
[16] B. Krause, C. Barbier, J. Levente, M. Klaus, P. Pötschke, Screening of Different Carbon Nanotubes in Melt-Mixed Polymer Composites with Different Polymer Matrices for Their Thermoelectrical Properties, J. Compos. Sci. 3 (2019) 106. https://doi.org/10.3390/jcs3040106.
[17] A.J. Lovinger, H.D. Keith, Electron Diffraction Investigation of a High-Temperature Form of Poly(vinylidene fluoride), Macromolecules. 12 (1979) 919–924. https://doi.org/10.1021/ma60071a026.
[18] W.M. Prest, D.J. Luca, The morphology and thermal response of high-temperature–crystallized poly(vinylidene fluoride), J. Appl. Phys. 46 (1975) 4136–4143. https://doi.org/10.1063/1.321438.
[19] W.M. Prest, D.J. Luca, The formation of the γ phase from the α and β polymorphs of polyvinylidene fluoride, J. Appl. Phys. 49 (1978) 5042–5047. https://doi.org/10.1063/1.324439.
[20] L. Li, M. Zhang, M. Rong, W. Ruan, Studies on the transformation process of PVDF from α to β phase by stretching, RSC Adv. 4 (2013) 3938–3943. https://doi.org/10.1039/C3RA45134H.
[21] V. Sencadas, R.G. Jr, S. Lanceros-Méndez, α to β Phase Transformation and Microestructural Changes of PVDF Films Induced by Uniaxial Stretch, J. Macromol. Sci. Part B. 48 (2009) 514–525. https://doi.org/10.1080/00222340902837527.
[22] H. Guo, Y. Zhang, F. Xue, Z. Cai, Y. Shang, J. Li, Y. Chen, Z. Wu, S. Jiang, In-situ synchrotron SAXS and WAXS investigations on deformation and α–β transformation of uniaxial stretched poly(vinylidene fluoride), CrystEngComm. 15 (2013) 1597–1606. https://doi.org/10.1039/C2CE26578H.
[23] J. Defebvin, S. Barrau, G. Stoclet, C. Rochas, J.-M. Lefebvre, In situ SAXS/WAXS investigation of the structural evolution of poly(vinylidene fluoride) upon uniaxial stretching, Polymer. 84 (2016) 148–157. https://doi.org/10.1016/j.polymer.2015.12.041.
[24] A.C. Lopes, C. Caparros, J.L. Gómez Ribelles, I.C. Neves, S. Lanceros-Mendez, Electrical and thermal behavior of γ-phase poly(vinylidene fluoride)/NaY zeolite composites, Microporous Mesoporous Mater. 161 (2012) 98–105. https://doi.org/10.1016/j.micromeso.2012.05.019.
[25] B.S. Ince-Gunduz, R. Alpern, D. Amare, J. Crawford, B. Dolan, S. Jones, R. Kobylarz, M. Reveley, P. Cebe, Impact of nanosilicates on poly(vinylidene fluoride) crystal polymorphism: Part 1. Melt-crystallization at high supercooling, Polymer. 51 (2010) 1485–1493. https://doi.org/10.1016/j.polymer.2010.01.011.
[26] A.C. Lopes, C.M. Costa, C.J. Tavares, I.C. Neves, S. Lanceros-Mendez, Nucleation of the Electroactive γ Phase and Enhancement of the Optical Transparency in Low

Filler Content Poly(vinylidene)/Clay Nanocomposites, J. Phys. Chem. C. 115 (2011) 18076–18082. https://doi.org/10.1021/jp204513w.
[27] M. El Achaby, F.Z. Arrakhiz, S. Vaudreuil, E.M. Essassi, A. Qaiss, Piezoelectric β-polymorph formation and properties enhancement in graphene oxide – PVDF nanocomposite films, Appl. Surf. Sci. 258 (2012) 7668–7677. https://doi.org/10.1016/j.apsusc.2012.04.118.
[28] P. Martins, C.M. Costa, M. Benelmekki, G. Botelho, S. Lanceros-Mendez, On the origin of the electroactive poly(vinylidene fluoride) β-phase nucleation by ferrite nanoparticles via surface electrostatic interactions, CrystEngComm. 14 (2012) 2807–2811. https://doi.org/10.1039/C2CE06654H.
[29] C.M. Wu, M.H. Chou, Polymorphism, piezoelectricity and sound absorption of electrospun PVDF membranes with and without carbon nanotubes, Compos. Sci. Technol. 127 (2016) 127–133. https://doi.org/10.1016/j.compscitech.2016.03.001.
[30] S.K. Rath, S. Dubey, G.S. Kumar, S. Kumar, A.K. Patra, J. Bahadur, A.K. Singh, G. Harikrishnan, T.U. Patro, Multi-walled CNT-induced phase behaviour of poly(vinylidene fluoride) and its electro-mechanical properties, J. Mater. Sci. 49 (2014) 103–113. https://doi.org/10.1007/s10853-013-7681-2.
[31] H.M. Ning, N. Hu, T. Kamata, J.H. Qiu, X. Han, L.M. Zhou, C. Chang, Y. Liu, L.K. Wu, J.H. Qiu, H.L. Ji, W.X. Wang, Y. Zemba, S. Atobe, Y. Li, Alamusi, H. Fukunaga, Improved piezoelectric properties of poly(vinylidene fluoride) nanocomposites containing multi-walled carbon nanotubes, Smart Mater. Struct. 22 (2013) 065011. https://doi.org/10.1088/0964-1726/22/6/065011.
[32] G.H. Kim, S.M. Hong, Y. Seo, Piezoelectric properties of poly(vinylidene fluoride) and carbon nanotube blends: β-phase development, Phys. Chem. Chem. Phys. 11 (2009) 10506–10512. https://doi.org/10.1039/B912801H.
[33] C.A. Hewitt, A.B. Kaiser, S. Roth, M. Craps, R. Czerw, D.L. Carroll, Multilayered Carbon Nanotube/Polymer Composite Based Thermoelectric Fabrics, Nano Lett. 12 (2012) 1307–1310. https://doi.org/10.1021/nl203806q.
[34] C.A. Hewitt, A.B. Kaiser, M. Craps, R. Czerw, S. Roth, D.L. Carroll, Temperature dependent thermoelectric properties of freestanding few layer graphene/polyvinylidene fluoride composite thin films, Synth. Met. 165 (2013) 56–59. https://doi.org/10.1016/j.synthmet.2013.01.009.
[35] C.A. Hewitt, D.L. Carroll, Extrinsic properties affecting the thermoelectric power output of few layer graphene/polyvinylidene fluoride composite thin films, Synth. Met. 162 (2012) 2379–2382. https://doi.org/10.1016/j.synthmet.2012.12.003.
[36] Y. Xiao, W. Wang, X. Chen, T. Lin, Y. Zhang, J. Yang, Y. Wang, Z. Zhou, Hybrid network structure and thermal conductive properties in poly(vinylidene fluoride) composites based on carbon nanotubes and graphene nanoplatelets, Compos. Part Appl. Sci. Manuf. 90 (2016) 614–625. https://doi.org/10.1016/j.compositesa.2016.08.029.
[37] A.K. Menon, R.M.W. Wolfe, S.R. Marder, J.R. Reynolds, S.K. Yee, Systematic Power Factor Enhancement in n-Type NiETT/PVDF Composite Films, Adv. Funct. Mater. 28 (2018) 1801620. https://doi.org/10.1002/adfm.201801620.

[38] R.M.W. Wolfe, A.K. Menon, T.R. Fletcher, S.R. Marder, J.R. Reynolds, S.K. Yee, Simultaneous Enhancement in Electrical Conductivity and Thermopower of n-Type NiETT/PVDF Composite Films by Annealing, Adv. Funct. Mater. 28 (2018) 1803275. https://doi.org/10.1002/adfm.201803275.
[39] T.H. Lee, F.Y.C. Boey, K.A. Khor, On the determination of polymer crystallinity for a thermoplastic PPS composite by thermal analysis, Compos. Sci. Technol. 53 (1995) 259–274. https://doi.org/10.1016/0266-3538(94)00070-0.
[40] K. Nakagawa, Y. Ishida, Annealing effects in poly(vinylidene fluoride) as revealed by specific volume measurements, differential scanning calorimetry, and electron microscopy, J. Polym. Sci. Polym. Phys. Ed. 11 (1973) 2153–2171. https://doi.org/10.1002/pol.1973.180111107.
[41] A. Schönhals, F. Kremer, Analysis of Dielectric Spectra, in: F. Kremer, A. Schönhals (Eds.), Broadband Dielectr. Spectrosc., Springer Berlin Heidelberg, Berlin, Heidelberg, 2003: pp. 59–98. https://doi.org/10.1007/978-3-642-56120-7_3.
[42] M.S.P. Shaffer, X. Fan, A.H. Windle, Dispersion and packing of carbon nanotubes, Carbon. 36 (1998) 1603–1612. https://doi.org/10.1016/S0008-6223(98)00130-4.
[43] M.A. Bachmann, W.L. Gordon, J. l. Koenig, J.B. Lando, An infrared study of phase-III poly(vinylidene fluoride), J. Appl. Phys. 50 (1979) 6106–6112. https://doi.org/10.1063/1.325780.
[44] T. Boccaccio, A. Bottino, G. Capannelli, P. Piaggio, Characterization of PVDF membranes by vibrational spectroscopy, J. Membr. Sci. 210 (2002) 315–329. https://doi.org/10.1016/S0376-7388(02)00407-6.
[45] J. Wu, J.M. Schultz, F. Yeh, B.S. Hsiao, B. Chu, In-Situ Simultaneous Synchrotron Small- and Wide-Angle X-ray Scattering Measurement of Poly(vinylidene fluoride) Fibers under Deformation, Macromolecules. 33 (2000) 1765–1777. https://doi.org/10.1021/ma990896w.
[46] J. Severino, J.-M. Yang, L. Carlson, R. Hicks, Progression of alignment in stretched CNT sheets determined by wide angle X-ray scattering, Carbon. 100 (2016) 309–317. https://doi.org/10.1016/j.carbon.2016.01.005.
[47] S. Barrau, A. Ferri, A. Da Costa, J. Defebvin, S. Leroy, R. Desfeux, J.-M. Lefebvre, Nanoscale Investigations of α- and γ-Crystal Phases in PVDF-Based Nanocomposites, ACS Appl. Mater. Interfaces. 10 (2018) 13092–13099. https://doi.org/10.1021/acsami.8b02172.
[48] L. He, Q. Xu, C. Hua, R. Song, Effect of multi-walled carbon nanotubes on crystallization, thermal, and mechanical properties of poly(vinylidene fluoride), Polym. Compos. 31 (2010) 921–927. https://doi.org/10.1002/pc.20876.
[49] C. Min, X. Shen, Z. Shi, L. Chen, Z. Xu, The Electrical Properties and Conducting Mechanisms of Carbon Nanotube/Polymer Nanocomposites: A Review, Polym.-Plast. Technol. Eng. 49 (2010) 1172–1181. https://doi.org/10.1080/03602559.2010.496405.
[50] H.-L. Zhang, J.-F. Li, B.-P. Zhang, K.-F. Yao, W.-S. Liu, H. Wang, Electrical and thermal properties of carbon nanotube bulk materials: Experimental studies for the 328--958 K temperature range, Phys. Rev. B. 75 (2007) 205407. https://doi.org/10.1103/PhysRevB.75.205407.

[51] B. Russ, A. Glaudell, J.J. Urban, M.L. Chabinyc, R.A. Segalman, Organic thermoelectric materials for energy harvesting and temperature control, Nat. Rev. Mater. 1 (2016) 16050. https://doi.org/10.1038/natrevmats.2016.50.